ARTICLE

The Determination of PZC and Differential Capacitance Curve of Platinum-Alkaline Polymer Electrolyte Interfaces

Chen-Xi Liu [a,#], Ze-Ping Zou [a,#], Mei-Xue Hu [b], Yu Ding [a], Yu Gu [a], Shuai Liu [a], Wen-Jing Nan [a], Yi-Chang Ma [a], Zhao-Bin Chen [a], Dong-Ping Zhan [a], Qiu-Gen Zhang [a,*], Lin Zhuang [b,*], Jia-Wei Yan [a,*], Bing-Wei Mao [a,*]

[a] College of Chemistry and Chemical Engineering, Xiamen University, Xiamen 361005, Fujian, China
[b] College of Chemistry and Molecular Sciences, Wuhan University, Wuhan 430072, Hubei, China

Abstract

Alkaline polymer electrolyte (APE) is the core component of modern alkaline hydrogen and oxygen fuel cells, and its single ion conductor nature makes the "electrode/APE" interfaces different from the conventional "electrode/solution" interfaces in terms of ion distribution, electrical double layer structure and polarization behavior. Due to the complexity of the APE and the associated solid−solid interfaces, fundamental investigations are challenging and deeper understanding of the structures and properties of such interfaces is in the infant stage. In this work, we aim to investigate the double layer structure from the aspects of differential capacitance curve and potential of zero charge (PZC) at the electrode/QAPPT (quaternary ammonia poly(Nmethyl-piperidine-co-p-terphenyl) interface. Cyclic voltammetry, electrochemical impedance spectroscopy (EIS) and microelectrode-based immersion techniques were employed. The differential capacitance curves of Pt/QAPPT interfaces exhibited an asymmetric U-shaped feature with a minimum at the potential which is consistent with the PZTC measured by the immersion method. The capacitance raised less quickly on the negative than the positive sides of the PZTC. These results reflect the characteristics of the single ion conductor and role of alkaline polyelectrolytes in modifying the double layer structure of the electrode/APE interfaces.

Keywords: Alkaline polymer electrolyte; Microelectrode; Differential capacitance curve; Potential of zero charge; Double layer structure

1. Introduction

Alkaline anion exchange membrane fuel cell (AEMFC) is the most promising technology in terms of sustainable hydrogen-based energy utilization [1,2]. The structures and properties of the electrode/APE interfaces where reactions are taking place play pivotal important roles in the reaction kinetics and thus the performance of AEMFCs [3,4]. APE is a single ion conductor, in which only the OH^- anions can move freely while the cations are confined in the framework of the polymer with a limited degree of spatial flexibility; and its interface formed with the electrode is solid−solid like, which makes the interfacial structure complicated and different from those of conventional "electrode/solution" interfaces in terms of ion distribution and structure of the electrical

Received 15 March 2023; Received in revised form 25 April 2023; Accepted 2 June 2023
Available online 8 June 2023

[#]These authors contributed equally to this work.
* Corresponding author, Qiu-Gen Zhang, Tel.: (86-592)2188072, E-mail address: qgzhang@xmu.edu.cn.

* Corresponding author, Lin Zhuang, Tel.: (86-27)68788793, E-mail address: lzhuang@whu.edu.cn.
* Corresponding author, Jia-Wei Yan, Tel.: (86-592)2186862, E-mail address: jwyan@xmu.edu.cn.
* Corresponding author, Bing-Wei Mao, Tel.: +(86-592)2186862, E-mail address: bwmao@xmu.edu.cn.

https://doi.org/10.13208/j.electrochem.2303151

double layer. However, fundamental investigations of such interfaces are challenging, and most of the existing researches focused on the development of APE [5,6], and thus, deeper understanding of the structures and properties of such interfaces is still in the infant stage.

Differential capacitance of an electrochemical interface is an important property of the electrical double layer (EDL). The differential capacitance curve (differential capacitance as a function of applied potential) contains rich information about structural change of the electrical double layer due to such as ion adsorption. Potential of zero charge (PZC) is another intrinsic property of electrochemical interface and reflects the interfacial charge behavior. In the case that no interfacial charge transfer occurs, the PZC will correspond to the point where the truly free, electronic excess charge density on the metal surface equals zero [7,8]. Alternatively, when adsorption processes involving partial charge transfer occur at metal-electrolyte interface, the potential at which the sum of the free, electronic excess charge density and the charge density transferred by adsorption processes equals zero is defined as potential of zero total charge (PZTC). According to Gouy-Chapman-Stern (GCS) theory [9], the capacitance minimum of the differential capacitance curve in a dilute electrolyte solution is located at PZC (or PZTC). In this case, the PZC can be determined from the capacitance minimum. However, such a conclusion might not be directly applied to the electrode/APE interface and therefore independent measurements on PZC is necessary to understand the feature of the differential capacitance and its meaning to the structural change of the associated EDL.

Some sophisticated experimental strategies have been developed to determine the PZTC of platinum electrodes, including the uses of CO and N_2O as probe molecules [10,11], and detection of the water adsorption [12,13] by infrared spectroscopy. On the other hand, the PZTC of metal electrode can also be determined by the so-called immersion method initially developed based on dropping mercury electrodes developed by Czajkowski and coworkers [14]. By this method, a freshly prepared electrode is rapidly brought to contact with the electrolyte at a pre-applied potential, and the current required for charging the EDL is recorded. The PZTC is then spotted at the potential with sign change of the charging current. This technique appears to be simple and has been mostly used in an aqueous solution [15] and ionic liquid systems [16—18] since it was proposed. Some PZTC values of dilute aqueous electrolyte solutions obtained by the differential capacitance minimum are in excellent agreement with the PZTC values obtained by immersion technique. The PZTC values of Au(111) [15] and Pt(111) [19,20] in $HClO_4$ solutions obtained by the above mentioned methods were also in excellent agreement with the minimum of the corresponding differential capacitance curve. However, most of the methods developed for aqueous electrolyte solutions cannot be used directly for determining the PZTC of electrode/polyelectrolyte interfaces due to the challenges brought by the illiquidity of the polyelectrolyte.

In this work, we employed Pt microelectrodes for investigation of the electrical double layer of Pt/APE interfaces, based on the measurements of differential capacitance curve and PZTC. The use of microelectrodes ensures good contact between the electrode and the solid-polymer electrolyte; and the impedance contribution from the microelectrode is assumed to be dominant compared to that of the much bigger counter electrode. The fitted capacitance value as a function of potential is U-shaped and the curve exists a minimum at potential which is consistent with the PZTC measured by the microelectrode-based immersion technique. The asymmetric feature of the U-shaped differential capacitance curve, with capacitance rising less quickly on the negative than the positive sides of the PZTC, disclosed the nature of the single ion conductor of anion polyelectrolyte. Our work demonstrated the advantageous of microelectrode for studying the electrode/polyelectrolyte interfaces and verified that the PZTC is located near the capacitance minimum of such interfaces.

2. Experimental

2.1. Materials

Potassium hydroxide (KOH) and sulfuric acid (H_2SO_4) were purchased from Sinopharm Chemical Reagents Co., Ltd. The APE employed in this work was quaternary ammonia poly(Nmethyl-piperidine-co-p-terphenyl) (QAPPT) polyelectrolyte provided by EVE Institute [21], and the related parameters are shown in Table 1.

Table 1. Basic parameters of anion exchange membrane QAPPT.

QAPPT	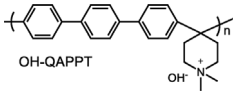
Ion exchange capacity (IEC)	2.50 ± 0.05 mmol·g^{-1}
Ionic conductivity	140 ± 10 mS·cm^{-1} @ 80 °C
Tensile strength	33 ± 3 MPa@R.T.
Thickness	50 μm
Counterpart ion	OH^-

Two differently grafted QAPPT membranes, i.e., 95% and 75% of grafting, were employed for electrochemical measurements. The grafting degree indirectly reflects the anion concentration in an APE membrane, and lower grafting degree corresponds to lower anion concentration. Deionized water (18.2 MΩ·cm, Milli-Q, Millipore) was used throughout the work.

2.2. The pretreatment process of anion exchange membrane

For ion exchange to OH^- form, the QAPPT membranes were immersed in 1 $mol \cdot L^{-1}$ KOH solution at 60 °C for 24 hours and then washed with deionized water for several times until the rinse water was neutral. The membrane was stored in 0.1 $mol \cdot L^{-1}$ KOH.

2.3. Preparation of Au-AuO_x quasi-reference electrode

Au-AuO_x electrode was prepared by potentiostatic polarization. The preparation procedures are outlined as follows:

① Soak a polycrystalline Au cylinder (3.58 mm in diameter) in piranha solution ($V_{H_2SO_4} : V_{H_2O_2} = 7 : 3$) overnight, clean it with deionized water and dry it.
② Prior to potentiostatic polarization, the Au cylinder (3.58 mm in diameter) electrodes were polished with 1, 0.3, and 0.05 μm alumina sequentially, washed with deionized water, and finally dried with Ar gas flow.
③ The Au cylinder was used as the working electrode, gold wire as the counter electrode, and the electrolyte used was 0.5 $mol \cdot L^{-1}$ H_2SO_4 solution. The potential was kept constant at 3.6 V for 15 minutes until the surface of the Au cylinder turned to reddish brown.

2.4. Electrochemical measurements

All electrochemical measurements were carried out using a Metrohm Autolab electrochemical workstation. A home-built three-electrode electrochemical cell made of PTFE was assembled and used for cyclic voltammetric (CV) and electrochemical impedance spectroscopic (EIS) measurements. A schematic view of the membrane electrode assembly (MEA) type of electrochemical cell is shown in Fig. 1(a). The cell consisted of a 25 μm Pt microelectrode or 3.58 mm Pt disk electrode, a carbon paper as the counter electrode placed on a serpentine flow channel, and the QAPPT membrane was sandwiched between them. The distance between the working and reference electrodes was kept short to reduce uncompensated IR resistance. Prior to the electrochemical measurement, the polycrystalline Pt electrode was polished successively with 1, 0.3, and 0.05 μm alumina powders, washed with deionized water, and finally dried with Ar gas flow. The EIS measurements were conducted as a function of potential within a frequency range from 10^5 to 0.1 Hz with an amplitude of 10 mV.

All of the measurements were performed at room temperature, and the electrochemical cell was placed in a Faraday cage to screen external electromagnetic noises. Prior to measurements, humidified Ar was fed to the cell for 1 hour. The Ar gas penetrated through the polyelectrolyte membrane to the working electrode. All potentials were initially measured versus the Au/AuO_x

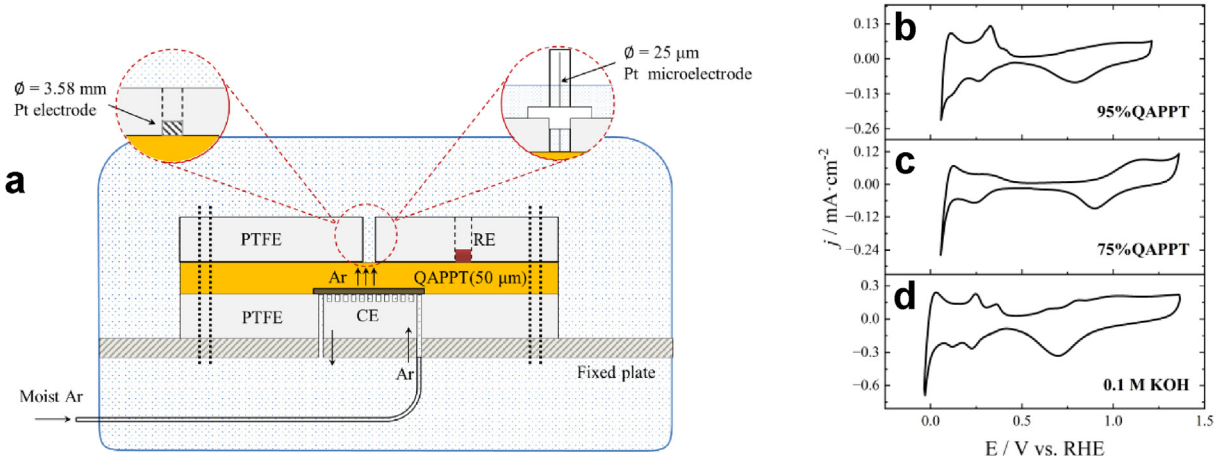

Fig. 1. (a) Experimental set-up to conduct electrochemical measurements for polyelectrolyte system; CV curves of polycrystalline Pt electrode (diameter 3.58 mm) contacted with 95%-grafted (b) and 75%-grafted (c) QAPPT membranes, and 0.1 mol·L^{-1} KOH solution (d). Sweep rate: 100 mV·s^{-1}.

quasi-reference electrode (in contact with a solid-polymer membrane) or a commonly used Hg/HgO reference electrode (used in aqueous electrolyte solutions). The potential of the Au/AuO_x electrode in contact with a specific QAPPT was calibrated against the Hg/HgO reference electrode. However, to avoid possible measurement error introduced during the calibration procedure or brought by the variation of the Au/AuO_x in potential, the hydrogen oxidation and evolution reactions (HOR/HER) in the corresponding QAPPT were directly taken to serve as an internal reference; a CV test was performed after the completion of each EIS or PZC measurement to determine the potential of the internal reference against the Au/AuO_x quasi-reference electrode. The potentials quoted in the text are versus such an internal reference electrode, i.e., RHE of the system under investigation, unless otherwise stated.

2.5. Immersion technique based on microelectrode

The immersion technique was carried out using a Metrohm Autolab electrochemical workstation. Before the measurement, a home-made 25 μm Pt microelectrode [22] was subjected to quick flame annealing followed by cooling under Ar atmosphere. Carbon paper and AuO_x/Au were used as the counter electrode (CE) and reference electrode (RE), respectively. The Pt microelectrode was rapidly brought to contact with the solid-polymer electrolyte at a pre-applied potential, and the corresponding current for charging the EDL was recorded. Charge vs. potential curve was constructed and potential of zero total charge was then obtained by linear fitting of the charge vs. potential plot near the region of charge polarity inversion, refer to the supplementary information.

3. Results and discussion

3.1. Cyclic voltammograms

Fig. 1(b), (c), and (d) shows the cyclic voltammograms (CVs) recorded under Ar atmosphere at the Pt disk electrode (3.58 mm in diameter) contacted with two kinds of grafted QAPPTs, 95% and 75%, and 0.1 mol·L^{-1} KOH solution, respectively. According to Fig. 1 (b) and (c), the CVs of QAPPTs remain normal, showing a small IR drop, even under the relatively fast scan rate of 100 mV $second^{-1}$. Furthermore, comparing the CVs of the same Pt disk electrode in QAPPT and KOH solution, they share similar characteristics but also with remarkable differences. On one hand, both voltammograms exhibit features similar to those of polycrystalline Pt electrodes in alkaline medias [23,24], which validates that the experimental approach for electrochemical measurements in polyelectrolyte is reliable and accurate. On the other hand, the detailed electrochemical behaviors of Pt electrode at QAPPT membrane are rather different from that in liquid electrolyte.

In terms of current density, the two kinds of grafted QAPPT membranes are smaller than KOH solution. In the hydrogen adsorption region, the currents associated with hydrogen adsorption and desorption peaks are lower than those in KOH solution, which may be related to the adsorption of the toxic residual I^- introduced during the synthesis of QAPPT [21,25,26]. In the double-layer region, the charging current in QAPPT is also smaller than that in the liquid KOH electrolyte. The reasons for the smaller current observed in QAPPT could be two-folded: On one hand, the areal density of the effectively mobile OH^-in the polymer framework is usually much lower than that in the 0.1 mol·L^{-1} KOH solution, which is a common drawback of polymer electrolytes including Nafion [2]. On the other hand, the contact of solid/polymer electrolyte interface is less sufficient than that of solid/solution interface because of the illiquidity of polyelectrolytes, which reduces the actual surface area accessible to the polyelectrolyte.

Interestingly, the 75%-grafted QAPPT has a wider double-layer potential range than the 95%-grafted QAPPT, noting that the former is supposed to be lower in areal density of the OH^- than the latter. Another significant difference between the CVs in the two kinds of electrolytes lie in the surface oxidation region. Compared to the KOH solution, the feature of the surface oxidation process in QAPPT is less resolvable.

3.2. Differential capacitance curve at Pt/QAPPT interfaces

As demonstrated in Fig. 2(a), for the 95%-grafted QAPPT, within the potential range from 0.4 V to 0.85 V vs. RHE, the current is non-Faradaic in nature, and hence may be considered as double layer region. Accordingly, the EIS measurements were performed at intervals of 50 mV within the above potential window. The use of microelectrode can effectively reduce the impedance interference from the counter electrode.

According to the Bode plot obtained at 0.76 V in Fig. 2(b), there are two obvious transitions in the frequency range between 1 Hz and 2500 Hz, corresponding to two interfacial processes. Therefore, two capacitance processes need to be introduced in the construction of electric equivalent circuits. To show more clearly the two capacitive processes, a complex capacitance plot is adopted. In such a

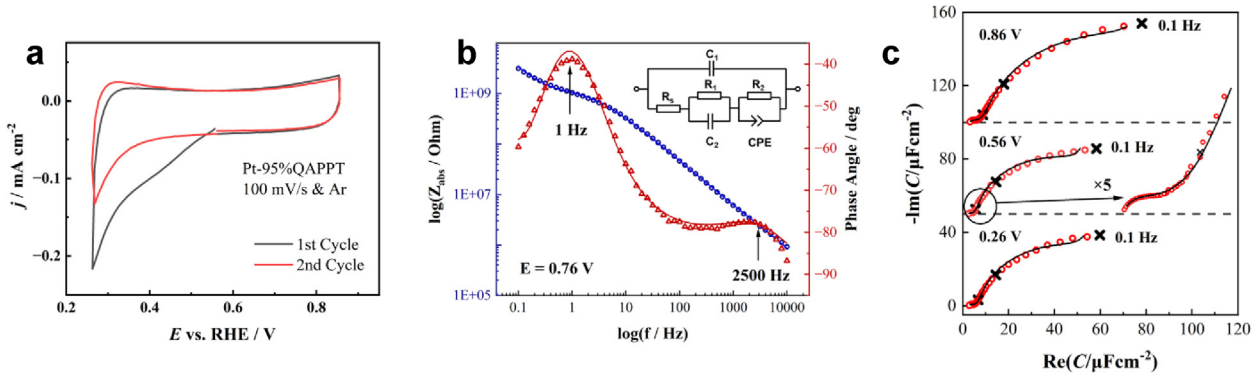

Fig. 2. (a) Cyclic voltammograms obtained at the 25 μm Pt microelectrode contacted with 95%-grafted QAPPT in Ar protection with a sweep rate of 100 mV second^{-1}. (b) Impedance spectra measured at E = 0.76 V vs. RHE. Solid lines are the fitted spectra, calculated according to the equivalent circuit shown in the inset. For the meaning of its elements, see the text. (c) Complex capacitance plots at the potentials indicated. The 10 Hz, 1 Hz, and 0.1 Hz points are marked by crosses; the solid lines are the fitted curves according to the equivalent circuit. The spectra are shifted along the ordinate for visibility reasons.

representation, two arcs are identifiable as shown in Fig. 2(c).

Considering the existence of bulk membrane resistance, parasitic capacitance caused by wires of the electrochemical workstation and interfacial dispersion behavior, an equivalent circuit shown in the inset of Fig. 2(b) was finally adopted to fit the measured impedance spectra. The equivalent circuit consists of two RC parallel circuits connected in series. Each RC circuit corresponds to a relaxation process, which is consistent with the two-arc structure in Fig. 2(b). The first RC parallel circuit pertains to the membrane itself and is representative of the membrane relaxation process; the second RC circuit is linked to the interfacial behavior at the Pt/QAPPT interface.

Impedance spectra within the potential between 0.26 V and 0.86 V were analyzed by fitting the parameters of the equivalent circuit to the measured spectra by a non-linear least squares program using modulus weighting, yielding parameters such as the bulk membrane resistance and double layer capacitance. The χ^2 values (residual mean squares) of the fits were in the order of 10^{-4}, indicating that the curve fitting is adequate. The constant phase element (CPE) components in equivalent circuits are associated with two main parameters: the admittance constant (Y_0) and adjustable factor (n). In almost full range of potential being investigated, the n values are greater than 0.8, indicating that it represents the capacitive element under certain frequency dispersion. The effective capacitance of the interface without Faraday reaction can be obtained by using the formula derived by Brug and coworkers for calculating the effective capacitance of CPE [27]:

$$C_{eff} = Y_0^{\frac{1}{n}} \cdot R_S^{\frac{1}{n}-1}$$

where C_{eff} is the effective capacitance of CPE, and R_s is the bulk membrane resistance.

The product of the resistance R and capacitance C is the relaxation time τ. It quantifies the speed of the capacitive process responding to a potential change. The shorter the time, the faster the response. Based on the Bode and complex capacitance plots in Fig. 2(b) and (c), the longer relaxation time corresponds to the membrane itself and is representative of the membrane relaxation process; the smaller one is linked to the interfacial capacitance behavior at the Pt/QAPPT interface. The fitted capacitance and n values as a function of potential are plotted in Fig. 3(a) for the 95%-grafted QAPPT system.

As shown in Fig. 3(a), the interfacial capacitance of the 95%-grafted QAPPT system shows a remarkable potential dependence in the range of measurement. The differential capacitance curve of the Pt/APE interface is U-shaped, and the potential of capacitance minimum is at 0.51 ± 0.06 V. The differential capacitance increases monotonically at both sides of the capacitance minimum, but much slower on the negative side than on the positive side of the capacitance minimum. In addition, the differential capacitance is smaller than that in aqueous solutions, which is, for example, about 20 μF·cm^{-2} in NaF solution reported by Pajkossy and Kolb [28] from impedance and capacitance measurements. This may be understood from two aspects: one is the illiquidity of polyelectrolytes, which reduces the actual surface area accessible to the polyelectrolyte; the other is the intrinsic difference in the charging and discharging capability between solid polyelectrolytes and liquid solutions.

To further inspect the influence of ion concentration, we also performed the same measurements for the 75%-grafted QAPPT, in which the OH^- concentration is supposed to be lower than

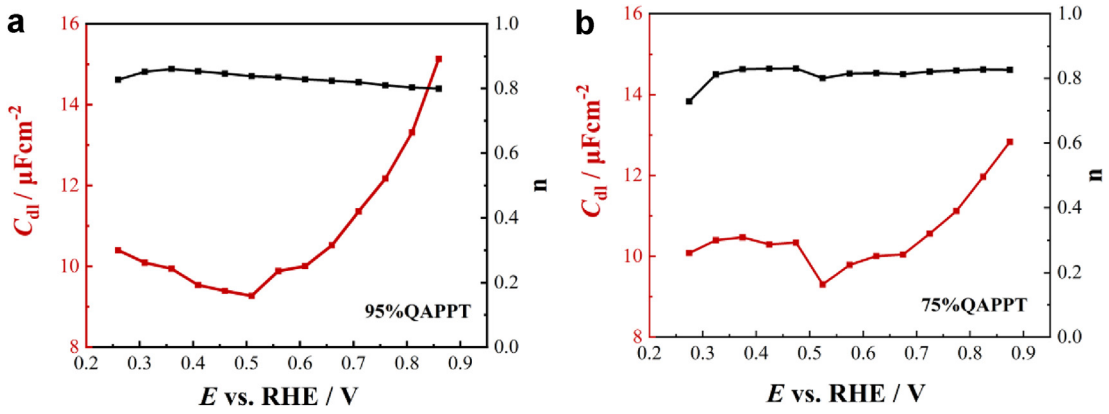

Fig. 3. The fitted capacitance and n values of the CPE as a function of potential, according to the proposed equivalent circuit shown in Fig. 2(b) with (a) 95%-grafted QAPPT and (b) 75%-grafted QAPPT. The potentials in both (a) and (b) are versus the RHE of the 95%-grafted QAPPT system.

that that in the 95%-grafted QAPPT. For the sake of easy comparison, the potential of the 75%-grafted QAPPT system is corrected against RHE of the 95%-grafted QAPPT system. As shown in Fig. 3(b) the capacitance curve of 75%-grafted QAPPT system shows similar U-shaped feature and the potential of the capacitance minimum is at 0.52 ± 0.05 V. The abrupt dropping in the capacitance and *n* values at the negative end of potential is likely caused by the Faradaic processes involved during the impedance measurement.

3.3. Potential of zero total charge at Pt/APE interfaces

To verify whether the capacitance minimum is in accordance with the PZTC, we further measured the PZTC of the QAPPT systems. Compared to liquid electrolytes, the complexity of the solid-polymer electrolyte brings many difficulties in the determination of PZTC [29,30]. While significant efforts have been put into improving the properties of APE, typically the stability and ionic conductivity, less work has been carried out in understanding the structure and property of the electrode/APE interfaces, such as potential of zero total charge [31–33]. In the present study the microelectrode-based immersion method was developed to get an idea about the PZTC of the electrode/polymer electrolyte interfaces.

In this method, the 25 μm Pt microelectrode after flame annealing was mounted in the PTFE cell and connected to an electrochemical workstation as the working electrode. After checking that the polymer electrolyte was in well contact with the reference and counter electrodes, the microelectrode was brought to contact with the polymer electrolyte, and the contacting procedure lasted for roughly 1 second. The current transient was recorded over several minutes, including the period of the contacting procedure. Unlike for the case of measurements in aqueous solutions, the transient current decayed slowly to zero. In addition, as the charge was obtained by integration, it depended on the duration of the experiment. As demonstrated in Fig. 4(b), the integrated charges calculated with the

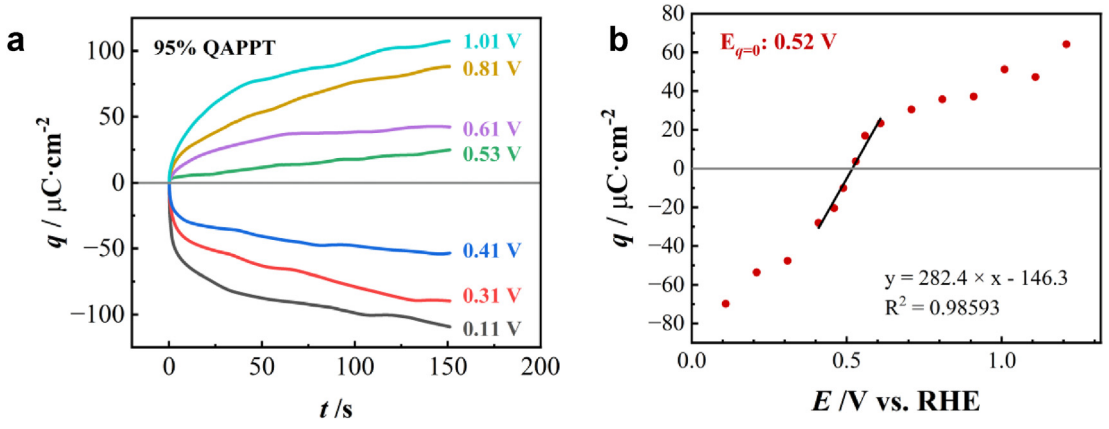

Fig. 4. (a) Integrated immersion charge transients of Pt microelectrode at the pre-set potentials in 95%-grafted QAPPT and (b) the charge integrated up to 5τ as a function of potential.

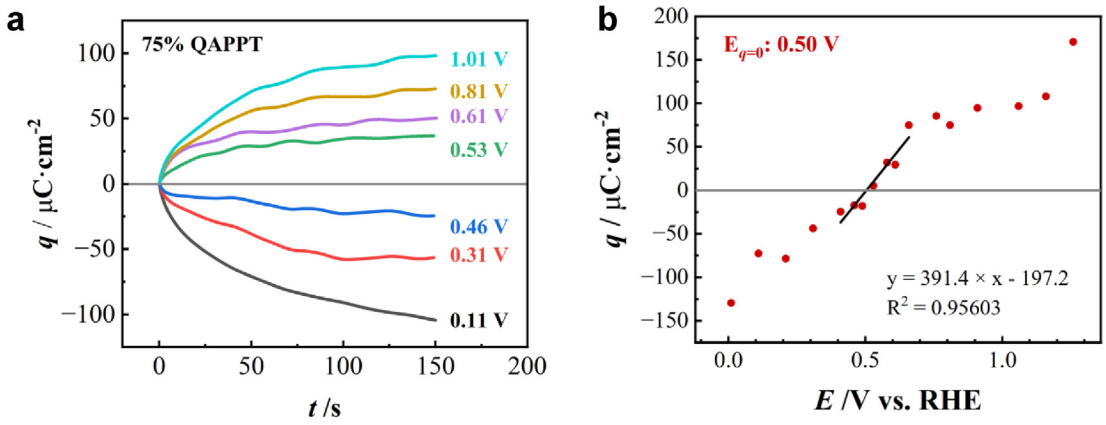

Fig. 5. (a) Integrated immersion charge transients of Pt microelectrode at the pre-set potentials in 75%-grafted QAPPT and (b) the charge integrated up to 5τ as a function of potential. The RHE of 95%-grafted QAPPT system is adopted.

first 5τ are plotted as a function of the immersion potential. The charge versus potential plot near the region of charge polarity inversion may be linearized, as shown by the solid line, and the potential at the zero charge crossing marks the PZTC, which is around 0.52 V *vs.* RHE. The value of PZTC agrees with the potential of the minimum of differential capacitance curve in Fig. 3(a).

However, under the tolerance of experimental measurement error, this value is roughly 150 mV lower than that at Pt(111)/NaOH interfaces at pH of 12.3 [34], that is close to the nominal pH of the 95%-grafted QAPPT. According to literature, the PZTC in aqueous solutions is negatively shifted along with the increase of solution pH [34–36]. But the actual OH^- concentration in the QAPPT is reduced due to the fact that the I^- introduced in the quaternary ammonium functionalized process of QAPPT membrane cannot be completely exchanged to OH^- during the pretreatment of the QAPPT membrane and that the CO_2 in the environment inevitably causes partial carbonation of OH^- in the membrane. Therefore, the lowering of the PZTC at the Pt/QAPPT interface likely arises from the single ion conductor nature of APE, making the "electrode/APE" interfaces electrochemically different from the conventional "electrode/solution" interfaces, and the microscopic mechanism for the discrepancy requires further exploration though.

The PZC measurement was also performed for the 75%-grafted QAPPT. As demonstrated in Fig. 5(b), the zero-cross in the case of 75%-grafted QAPPT is also at around 0.50 V *vs.* RHE (95%-grafted QAPPT), which is again in agreement with the potential of capacitance minimum of the system.

We therefore presume that the PZTC at the electrode/solid-polymer electrolyte interface is located near the capacitance measurement within the tolerance of measurement errors. The U-shaped asymmetric differential capacitance curve across the PZTC reveals the asymmetric polarization behavior of the Pt/QAPPT interfaces, which is weaker on the negative side compared to the positive side. This asymmetric feature clearly reflects the nature of anion-type of single ion conductors in constraining the motion of cations, which results in the thickening of the electric double layer in the polymer side of the interface and thus the reduction of differential capacitance values at potentials negative of the PZTC. On the other hand, there are almost no differences in the potential of capacitance minimum and the PZTC between 95%-grafted and 75%-grafted QAPPT systems. But given that theoretically the difference of OH^- content in the two QAPPT membranes is no more than two times, the meaning of the apparent invariance of PZTC of the two differently grafted QAPPT systems remains to be further explored and understood.

4. Conclusions

In summary, we have employed microelectrodes to study the electrochemical behaviors of Pt/QAPPT interfaces based on electrochemical impedance spectroscopy and immersion technique. The capacitance curves exhibit U-shaped features, and exist minimum at the potential which is consistent with the corresponding PZTC measured by microelectrode-based immersion technique. The asymmetric differential capacitance curve with the capacitance rising less quickly on the negative than positive sides of the PZTC reflects the nature of the single ion conductor of alkaline polymer electrolyte (APE). These results disclose the profound role of the APE as a single ion conductor in modifying the structure of the double layer of the electrode/electrolyte interfaces.

The microelectrode-based immersion method can also be extended to study the PZC of other polymer electrolyte systems. However, to fully understand the structures and processes of the electrode/polyelectrolyte interfaces, future studies could be carried out in the following two aspects. On one hand, experiments employing QAPPT with much lower grafting degrees should be conducted to further clarify the concentration influence of ions on the PZC. On the other hand, other non-electrochemical techniques such as vibrational spectroscopy are necessary to obtain molecular level structural information at the interfaces.

Acknowledgements

This work was supported by the National Natural Science Foundation of China (Nos. 21991150/1, 21972119 and 22002129). The authors thank Professors Jun Cheng and Xiao-Hui Yang at the Xiamen University for the helpful discussion, and Yang Wang at the Xiamen University for the assistance of microelectrode preparation.

References

[1] Wang Y J, Qiao J L, Baker R, Zhang J J. Alkaline polymer electrolyte membranes for fuel cell applications[J]. Chem. Soc. Rev., 2013, 42(13): 5768−5787.

[2] Varcoe J R, Atanassov P, Dekel D R, Herring A M, Hickner M A, Kohl P A, Kucernak A R, Mustain W E, Nijmeijer K, Scott K, Xu T, Zhuang L. Anion-exchange membranes in electrochemical energy systems[J]. Energy Environ. Sci., 2014, 7(10): 3135−3191.

[3] Kusoglu A, Weber A Z. New insights into perfluorinated sulfonic-acid ionomers[J]. Chem. Rev., 2017, 117(3): 987−1104.

[4] Ramaswamy N, Mukerjee S. Alkaline anion-exchange membrane fuel cells: Challenges in electrocatalysis and interfacial charge transfer[J]. Chem. Rev., 2019, 119(23): 11945−11979.

[5] Wang L, Bellini M, Miller H A, Varcoe J R. A high conductivity ultrathin anion-exchange membrane with 500+ H alkali stability for use in alkaline membrane fuel cells that can achieve 2 $W \cdot cm^{-2}$ at 80 °C[J]. J. Mater. Chem. A, 2018, 6(31): 15404−15412.

[6] Du X M, Zhang H Y, Yuan Y J, Wang Z, Xu J M. Synthesizing spindle-shaped anion exchange membranes to improve conductivity and stability[J]. Int. J. Hydrogen Energy, 2020, 45(20): 11814−11823.

[7] Frumkin A N, Petrii O A. Potentials of zero total and zero free charge of platinum group metals[J]. Electrochim. Acta, 1975, 20(5): 347−359.

[8] Kolb D M. Book review: Comprehensive treatise of elec trochemistry. vol. 1. In: Bockris J O'm, Conway B E, Yeager E, editors. The double layer [J]. Angew. Chem. Int. Ed. 1981, 20: 817−818.

[9] Zha Q X. The introduction of electrode process kinetics[M]. second ed. Beijing: Science Press, 2002.

[10] Attard G A, Ahmadi A. Anion—surface interactions Part 3. N_2O reduction as a chemical probe of the local potential of zero total charge[J]. J. Electroanal. Chem., 1995, 389(1): 175−190.

[11] Cuesta A. Measurement of the surface charge density of CO-saturated Pt(111) electrodes as a function of potential: The potential of zero charge of Pt(111)[J]. Surf. Sci., 2004, 572(1): 11−22.

[12] Silva C D, Cabello G, Christinelli W A, Pereira E C, Cuesta A. Simultaneous time-resolved ATR-SEIRAS and CO-charge displacement experiments: The dynamics of CO adsorption on polycrystalline Pt[J]. J. Electroanal. Chem., 2017, 800: 25−31.

[13] Iwasita T, Xia X. Adsorption of water at Pt(111) electrode in $HClO_4$ solutions. The potential of zero charge[J]. J. Electroanal. Chem., 1996, 411(1): 95−102.

[14] Czajkowski J M, Blaszczyk T, Kazmierczak D. Automatic-apparatus for precise measuring and recording of PZC value of liquid electrodes and its application[J]. Electrochim. Acta, 1984, 29(4): 439−443.

[15] Hamm U W, Kramer D, Zhai R S, Kolb D M. The PZC of Au(111) and Pt(111) in a perchloric acid solution: An ex situ approach to the immersion technique[J]. J. Electroanal. Chem., 1996, 414(1): 85−89.

[16] Gnahm M, Pajkossy T, Kolb D M. The interface between Au(111) and an ionic liquid[J]. Electrochim. Acta, 2010, 55(21): 6212−6217.

[17] Gnahm M, Muller C, Repanszki R, Pajkossy T, Kolb D M. The interface between Au(100) and 1-butyl-3-methyl-imidazolium-hexafluorophosphate[J]. Phys. Chem. Chem. Phys., 2011, 13(24): 11627−11633.

[18] Müller C, Vesztergom S, Pajkossy T, Jacob T. Immersion measurements of potential of zero total charge (Pztc) of Au(100) in an ionic liquid[J]. Electrochim. Acta, 2016, 188: 512−515.

[19] Ojha K, Arulmozhi N, Aranzales D, Koper M TM. Double layer at the Pt(111)-aqueous electrolyte interface: Potential of zero charge and anomalous gouy-chapman screening[J]. Angew. Chem. Int. Ed., 2020, 59(2): 711−715.

[20] Ojha K, Doblhoff-Dier K, Koper M TM. Double-layer structure of the Pt(111)-aqueous electrolyte interface[J]. Proc. Natl. Acad. Sci. U.S.A., 2022, 119(3): e2116016119.

[21] Peng H Q, Li Q H, Hu M X, Xiao L, Lu J T, Zhuang L. Alkaline polymer electrolyte fuel cells stably working at 80 °C[J]. J. Power Sources, 2018, 390: 165−167.

[22] Ma Z, Lin J Y, Nan W J, Han L H, Zhan D P. Ultramicroelectrode experiments: Principles, fabrications and voltmmetric behaviors[J]. J. Electrochem. 2022 1006-3471(2022)00-0000-00.

[23] Ramaswamy N, Mukerjee S. Influence of inner- and outer-sphere electron transfer mechanisms during electrocatalysis of oxygen reduction in alkaline media[J]. J. Phys. Chem. C, 2011, 115(36): 18015−18026.

[24] Liao L W, Li M F, Kang J, Chen D, Chen Y X, Ye S. Electrode reaction induced pH change at the Pt electrode/electrolyte interface and its impact on electrode processes [J]. J. Electroanal. Chem., 2013, 688: 207−215.

[25] Podlovchenko B I, Kolyadko E A. Variations in the charge and open-circuit potential of a platinum electrode during adsorption of iodine and iodide ions[J]. Russ. J. Electrochem., 2000, 36(12): 1268−1274.

[26] Bagotzky V S, Vassilyev Y B, Weber J, Pirtskhalava J N. Adsorption of anions on smooth platinum electrodes[J]. J. Electroanal. Chem., 1970, 27(1): 31−46.

[27] Brug G J, van den Eeden A LG, Sluyters-Rehbach M, Sluyters J H. The analysis of electrode impedances complicated by the presence of a constant phase element[J]. J. Electroanal. Chem., 1984, 176(1): 275−295.

[28] Pajkossy T, Kolb D M. On the origin of the double layer capacitance maximum of Pt(111) single crystal electrodes[J]. Electrochem. Commun., 2003, 5(4): 283−285.
[29] Schuler T, Chowdhury A, Freiberg A T, Sneed B, Spingler F B, Tucker M C, More K L, Radke C J, Weber A Z. Fuel-cell catalyst-layer resistance via hydrogen limiting-current measurements[J]. J. Electrochem. Soc., 2019, 166(7): F3020−F3031.
[30] Srebnik S, Pusara S, Dekel D R. Effect of carbonate anions on quaternary ammonium-hydroxide interaction[J]. J. Phys. Chem. C, 2019, 123(26): 15956−15962.
[31] Hanawa H, Kunimatsu K, Watanabe M, Uchida H. *In Situ* ATR-FTIR analysis of the structure of nafion-Pt/C and nafion-Pt_3Co/C interfaces in fuel cell[J]. J. Phys. Chem. C, 2012, 116(40): 21401−21406.
[32] Ahmed M, Morgan D, Attard G A, Wright E, Thompsett D, Sharman J. Unprecedented structural sensitivity toward average terrace width: Nafion adsorption at Pt{Hkl} electrodes[J]. J. Phys. Chem. C, 2011, 115(34): 17020−17027.
[33] Park E J, Arges C G, Xu H, Kim Y S. Membrane strategies for water electrolysis[J]. ACS Energy Lett., 2022, 7(10): 3447−3457.
[34] Rizo R, Sitta E, Herrero E, Climent V, Feliu J M. Towards the understanding of the interfacial pH scale at Pt(111) electrodes[J]. Electrochim. Acta, 2015, 162: 138−145.
[35] Mello G AB, Briega-Martos V, Climent V, Feliu J M. Bromide adsorption on Pt(111) over a wide range of pH: Cyclic voltammetry and CO displacement experiments[J]. J. Phys. Chem. C, 2018, 122(32): 18562−18569.
[36] Xu P, von Rueden A D, Schimmenti R, Mavrikakis M, Suntivich J. Optical Method for Quantifying the potential of zero charge at the platinum-water electrochemical interface[J]. Nat. Mater., 2023, 22(4): 503−510.

电极/碱性聚电解质界面的微分电容曲线和零电荷电位测定

刘晨希[a,#]，邹泽萍[a,#]，胡梅雪[b]，丁　宇[a]，谷　宇[a]，刘　帅[a]，南文静[a]，马溢昌[a]，陈招斌[a]，詹东平[a]，张秋根[a,*]，庄　林[b,*]，颜佳伟[a,*]，毛秉伟[a,*]
[a]厦门大学化学化工学院，福建 厦门 361005
[b]武汉大学化学与分子科学学院，湖北 武汉 430072

摘要

碱性聚合物电解质作为现代碱性氢氧燃料电池的核心组成部分，其单离子导体的特性使得“电极/碱性聚电解质”界面的性质与“电极/溶液”界面有所不同。本文使用微电极，运用循环伏安、电化学交流阻抗以及浸入法等方法，测定了电极/碱性聚电解质界面的微分电容曲线和零电荷电位。该界面的微分电容曲线呈“U”状，且存在局域极小值，该极小值所对应的电位与浸入法测得的零电荷电位数值一致。单离子导体的特性使得“电极/碱性聚电解质”界面在零电荷电位两侧表现出不同的电化学极化行为。

关键字：碱性物电解质；双电层；微电极；微分电容曲线；零电荷电位